# Recognition and Reactivity in the Binding between Raf Kinase Inhibitor Protein and Its Small-Molecule Inhibitor Locostatin

Aleksandra N. Rudnitskaya, Nicholas A. Eddy, Gabriel Fenteany, and José A. Gascón*

Department of Chemistry, The University of Connecticut, 55 North Eagleville Road, Storrs, Connecticut 06269, United States

S Supporting Information

ABSTRACT: The present work is aimed to provide detail on the binding process between Raf kinase inhibitor protein (RKIP) and locostatin, the only exogenous compound known to alter the function of RKIP. Understanding the basis of RKIP inhibition for use in pharmacological applications is of considerable interest, as dysregulated RKIP expression has the potential to contribute to pathophysiological processes. Herein, we report a series of atomistic models to describe the protein−ligand recognition step and the subsequent reactivity steps. Modeling approaches include ligand docking, molecular dynamics, and quantum mechanics/molecular mechanics calculations. We expect that such a computational assay will serve to study similar complexes in which potency is associated with recognition and reactivity. Although previous data suggested a single amino acid residue (His86) to be involved in the binding of locostatin, the actual ligand conformation and the steps involved in the reactivity process remain elusive from a detailed atomistic description. We show that the first reaction step, consisting of a nucleophilic attack of the nitrogen (N_ε) of His86 at the sp^2-hybridized carbon (C2) of locostatin, presents a late transition state (almost identical to the product). The reaction is followed by a hydrogen abstraction and hydrolysis. The theoretically predicted overall rate constant ($6\ M^{-1}\ s^{-1}$) is in a very good agreement with the experimentally determined rate constant ($13\ M^{-1}\ s^{-1}$).
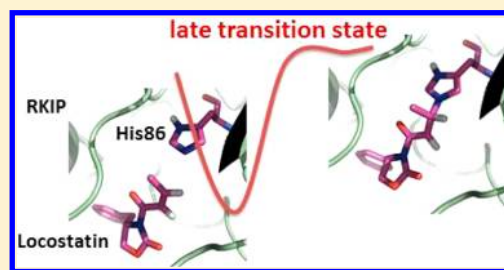
INTRODUCTION

Raf kinase inhibitor protein (RKIP) is a member of the phosphatidylethanolamine-binding protein (PEBP) family. It is an small, evolutionarily conserved cytosolic protein that plays a pivotal modulatory role in several protein kinase signaling cascades.[1−5] RKIP was originally identified as a protein that bound phosphatidylethanolamine[6] (although this interaction might be nonspecific)[7] and subsequently shown to be an endogenous regulator of Raf-1 kinase[1,8] and other kinases, including G protein-coupled receptor kinase 2 (GRK2)[3] and kinases involved in nuclear factor κB signaling.[2,4,9,10] In addition to its function in normal physiological phenomena, dysregulated RKIP expression has the potential to contribute to pathophysiological processes including Alzheimer's disease and diabetic nephropathy.[11−13] Intriguingly, RKIP has also been shown to fit the criteria of being a metastasis suppressor.[14−17] In fact, a number of different human cancers have been shown to be differentially regulated by RKIP. Therefore, RKIP might provide a useful predictive marker for tumor and tumor metastases tissues. RKIP might also be involved in immunotherapy against human cancer.[18]

It is relevant, therefore, to design a platform for building successful probes or biomarkers for RKIP to investigate its basic function. Producing better probes will aid in the effort of perturbing the function of RKIP potently and specifically to define its many and seemingly contradictory roles. In this work, we characterize the binding properties of locostatin, which is the only known RKIP inhibitor found to date.[19] Locostatin binds RKIP and prevents it from associating with Raf-1 kinase, thus functioning as an inhibitor of a critical protein−protein interaction in the regulation of Raf kinase pathway.[18] More recently, it was found that locostatin also prevents RKIP from associating with GRK2, another kinase that has been implicated in the control of cell migration.[20]

Locostatin contains a 2-oxazolidinone core connected to a crotonyl moiety by an amide bond. The presence of an α,β-unsaturated carbonyl functionality (Michael acceptor) makes locostatin potentially reactive toward nucleophiles. Regarding its action on RKIP, mass spectrometry studies showed that locostatin primarily alkylates a specific residue (His86).[20] Although locostatin binds RKIP with slow kinetics, after the event, the crotonyl group of locostatin slowly hydrolyzes from the oxazolidinone moiety, leaving an RKIP−butyrate complex (Figure 1).

Although all these previous studies suggested a single protein residue (His86) to be involved in the binding of locostatin, a full characterization of locostatin's mode of binding, its interaction with the protein cavity, and subsequent reactivity remain elusive for a detailed atomistic description. Moreover, locostatin tends to cause RKIP to partially aggregate in vitro, making it difficult to obtain NMR spectra or X-ray crystal structures.[20,21] Therefore, considering the lack of structural data, a full atomistic description is urgently needed for the future optimization and design of molecular probes for RKIP.
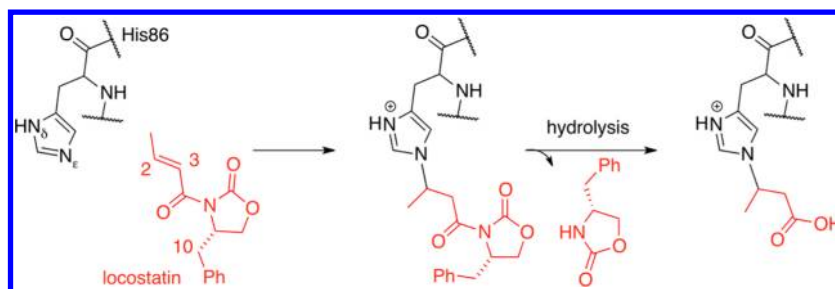
Figure 1. Mechanism of chemical modification of RKIP by locostatin at the His86 position and subsequent hydrolysis of the bound locostatin.

With this goal in mind, we implemented several levels of modeling to address these questions. First, molecular docking provided a number of possible conformers and relative orientations with respect to the cavity. Second, molecular dynamics (MD) simulations were carried out to determine the stability of selected docked poses and the likelihood that the reacting moieties of both locostatin and His86 are within appropriate distances for the reaction to take place. These two steps, docking and MD, can be regarded as mimicking the recognition step of locostatin by the protein cavity. Third, quantum mechanics/molecular mechanics (QM/MM) energy minimizations were employed to uncover the detailed reaction pathway, determine the energy profile for the entire reaction, and predict an overall rate constant.

COMPUTATIONAL METHODS

Docking. All computations were based on the X-ray crystal structure of the human Raf kinase inhibitor protein in complex with O-phosphotyrosine (PDB ID 2QYQ).[14] The PDB structure was processed with the protein preparation toolkit in Maestro (Schrodinger Inc.).[22] This toolkit assigns protonation states under the assumption of neutral pH. The amino acids' microenvironment is also taken into account for the assignment of protonation, tautomers, and side-chain conformers. Concerning the protein cavity, it is worth mentioning that protonation of His86 is at N_δ, whereas for the nearby His118, the program assigns a double protonation state because of its interaction with Asp70 and other hydrogen-bond acceptors (Pro74, Thr115).

To identify starting geometries of locostatin in solution (later used in docking), we generated a set of rotamers involving the first four bonds (from C1 to N6) (see Figure S1 in the Supporting Information for details). These structures were minimized using density functional theory at the B3LYP/6-31G** level with implicit water, treated in a conductor-like model. This step provided a subset of low-energy structures within a range of 3 kcal/mol from the lowest energy. Although the generation of rotamers was not exhaustive, the objective of selecting this low-energy family was to aid in the generation of docking poses, which was found to be slightly dependent on the starting geometry of the ligand. The program Glide 5.0[23] was used for docking, under rigid-receptor (flexible-ligand) conditions in standard-precision (SP) mode.[23−27] The binding site was defined by generating a grid with dimensions of 20.0 Å × 20.0 Å × 20.0 Å, centered on His86. The scaling factor for van der Waals radii was set at 0.8. To benchmark the algorithm within the context of RKIP, the cocrystallized phosphotyrosine ligand present in the 2QYQ structure was redocked and compared to the X-ray structure, returning a root-mean-square deviation of 0.37 Å, in excellent agreement with the original cocrystal conformation.

Docking of locostatin generated a highly diverse set of poses even within the top-ranked poses. This observation is already of relevance, as it suggests that locostatin can serve as a basis for the design of new ligands with improved specificity, which could eventually produce enzyme inhibition without covalent binding. The docking poses were characterized by different locostatin rotamers and by the relative orientation of the locostatin alkene group with respect to the cavity. To be unbiased in the selection of these poses, we chose a set of 18 poses reflecting a diverse set of conformations (descriptions of the 18 selected poses are presented in the Supporting Information). Each of these poses was reranked by computing their energies within a QM/MM approach using the program QSite.[28] Further refinement to select the best pose was carried out by combining three different criteria: (1) The pose must have the acyl group oriented toward the cavity (otherwise, the known reaction with His86 would not occur). (2) The pose must have a high docking score. (3) The pose must have a low single-point energy (SPE) according to QSite. The resulting refined pose, meeting all of these criteria in the best possible way, is shown in Figure 2. The conformation of locostatin in
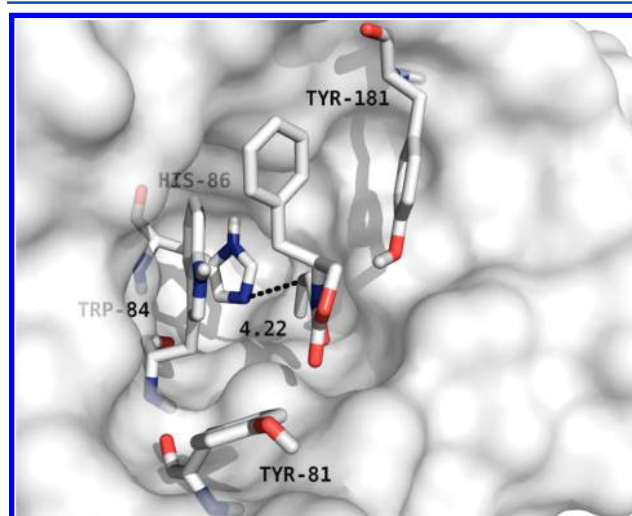

Figure 2. Top-ranked conformation of locostatin according to a combination of docking and QM/MM energy criteria.

this pose is characterized by the acyl group being oriented toward the cavity interior, leaving the benzene group barely outside the cavity. Furthermore, the distance between the C2 carbon of the α,β-unsaturated acyl group and the N_ε atom of His86 is 4.22 Å (Figure 2). Clearly, such a pose is potentially well situated to alkylate His86 and is expected to shorten further during finite-temperature simulations. It is also worth noticing that there is a structural similarity between locostatin

and the phosphotyrosine ligand in terms of the occupied volume (182 versus 195.0 Å^3, respectively) and that locostatin extends inside the cavity, occupying a volume similar to that occupied by phosphotyrosine (see Figure S3, Supporting Information).

Molecular Dynamics. MD simulations in the *NPT* ensemble were performed using the program Desmond, version 3.0.[29−31] The purpose of this MD simulation was two-fold: to determine the stability of the initial ligand pose over a time of several nanoseconds and to allow the protein cavity to adapt to the presence of locostatin. Indeed, this simulation gave rise to even shorter distances between the protein/ligand reacting groups, as compared to the one predicted by the rigid-protein/flexible-ligand docking procedure described previously. The initial structure of the RKIP−locostatin complex for MD was obtained according to the docking procedure (Figure 2). Water molecules were placed by soaking the system with a pre-equilibrated cubic water box having a buffer region of 10 Å from the outermost part of the protein. The system was neutralized with sodium ions. The TIP3P water model[32] was used for all simulations. After the system had been heated slowly to 300 K (total time of 1.2 ns, with a time step 100 ps and a temperature increment of 50 K), a 24-ns MD simulation was performed in an *NPT* ensemble at 300 K and 1 atm using a reversible system propagation algorithm (RESPA), a Nosé−Hoover thermostat, and a Martyna−Tobias−Klein barostat. Energy and atomic coordinate trajectory data were recorded every 4.8 ps.

Considerable changes emerged in the MD simulation. The most important was the rotation of the C4−N6 single bond, positioning the two neighboring oxygen atoms in a trans conformation (Figure 3). Such movement allowed the reacting
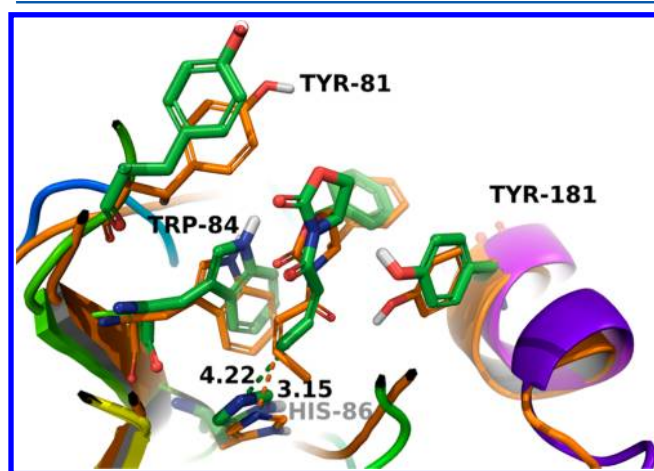

Figure 3. Reorganization of locostatin from docking (green sticks) to molecular dynamics (orange sticks).

C2 carbon to get considerable closer to the His N$_\varepsilon$ atom. Concomitant with this change, a significant movement of N$_\varepsilon$ toward the C2 atom of locostatin occurred. Overall, the C2−N$_\varepsilon$ distance shortened even further during MD, reaching a minimum distance of 3.15 Å. A question that remained to be answered was whether other poses could lead to qualitatively different conformations that could also favor a reaction. To answer this question, we tested other poses that were close to the best one selected according to the refinement criteria explained earlier. These poses differed in terms of the rotamers around the C2−C3 bond and the C4−N6 bond, which could

be in either cis or trans configuration. MD simulations starting from C2−C3 in the trans configuration (pose 5 in Figure S2, Supporting Information) ended up pulling locostatin away from His86. Thus, C2−C3 was left in the cis configuration. Also, starting from C4−N6 in the trans conformer (pose 3 in Figure S2, Supporting Information) ended up in a position very similar to that starting from cis, which, as already explained, rotated during the simulation. We conclude, therefore, that the MD simulation finally used for the subsequent QM/MM calculations represented a converged result.

QM/MM Study. QM/MM calculations were carried out to determine the energetics involved in the alkylation step and subsequent hydrolysis. The beginning structure was the result of the previous MD procedure. It was identified as the snapshot with the smallest distance between the nonprotonated nitrogen (N$_\varepsilon$) of His86 and the C2 of locostatin (3.15 Å). The QM region included locostatin, His86, and the residues adjacent to His86 (His85, Phe87). Density functional theory (DFT) calculations were performed using QSite at the B3LYP/6-31 g* level of theory. The rest of the protein was described according to the force field OplsAA.[33,34] Geometry optimization was carried out by freezing the entire protein except for a 5-Å buffer region around locostatin and His86. Solvation effects were taken into account through a Poisson−Boltzmann solvation term as implemented in Qsite.

■ RESULTS AND DISCUSSION

For the reactive steps following enzyme−substrate (**ES**) complexation, we propose a three-step mechanism (Scheme 1

Scheme 1. Proposed Pathways for the Reaction between Locostatin and His86 (RKIP), Resulting in the Formation of the Enzyme−Product Complex (EP)^a
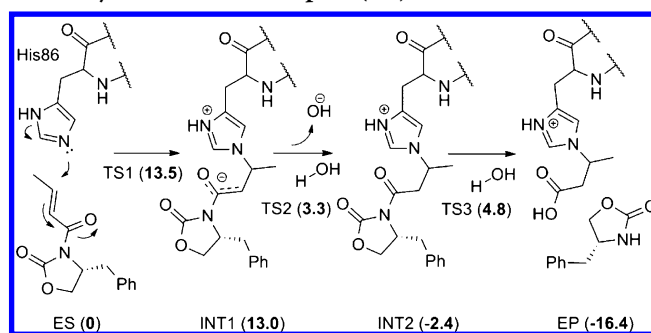
^{a}Numbers in parentheses are energies in kcal/mol computed with respect to the immediate reactant to the left.

and Figure 4). The first step is a nucleophilic attack of the imidazole N$_\varepsilon$ of His86 on the C2 of locostatin. **ES** produces the zwitterion **INT1** through a transition state (**TS1**) that is 13.0 kcal/mol above **ES**. On the reactive side, the QM/MM minimization results in a N$_\varepsilon$−C2 distance of 3.71 Å, whereas on the product side, the corresponding distance decreases to 1.57 Å, leading to a change in hybridization of C2. Furthermore, the transition state **TS1** is markedly closer in energy and structure to the product **INT1** (13.5 kcal/mol). Thus, the same factors that stabilize the product stabilize the transition state as well, and the two are interconverted with only a small reorganization of molecular structure. Although this is an extreme case of the so-called late transition state, such a feature is generally characteristic of slow endothermic reactions.
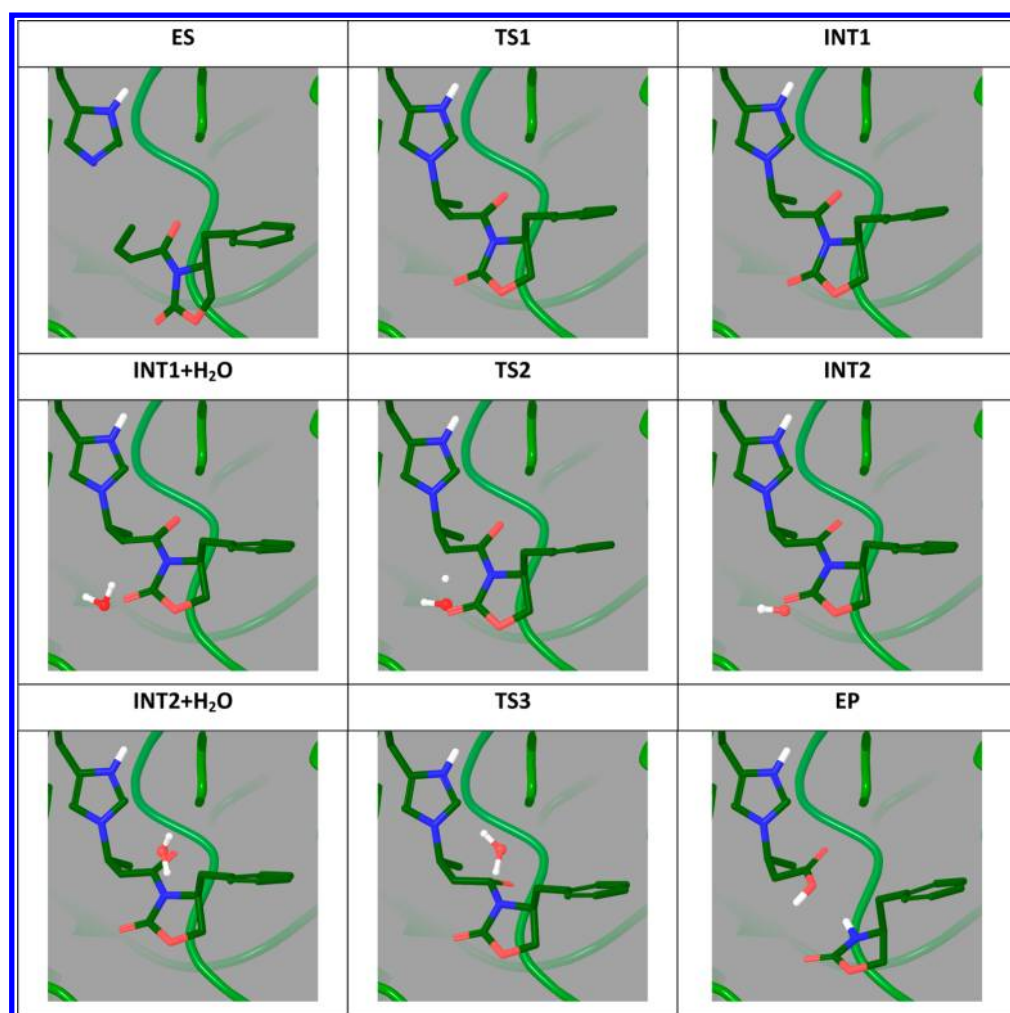
Figure 4. Reactants, transition states, and intermediate states optimized at the B3LYP/lacvp*:OPLS2005 level of theory.

The second step of the reaction involves hydrogen abstraction from a nearby solvent water molecule. The most reasonable scenario consists of a nucleophilic attack of the C3 carbon of the acyl group. Calculations of QM-derived charges showed that C3 is the most electronegative atom in **INT1**, carrying a charge of −0.72e, which supports the proposed scenario. Attack on C3 occurs through an activation barrier of 3.3 kcal/mol (**TS2**), producing an intermediate (**INT2**) that is 2.4 kcal/mol lower in energy than **INT1**. It was shown in previous experimental studies that the RKIP−locostatin complex slowly hydrolyzes to RKIP−butyrate. Thus, a second water was placed and optimized in a position suitable to the attack of C4. The enzyme−product (**EP**) complex, product of the hydrolysis, is 16.4 kcal/mol more stable than the reactant **INT2**. The transition state (**TS3**) between **ES** and **INT2** is 4.9 kcal/mol higher than the reactant **INT2**.

Having evaluated the energy profile according to the proposed mechanism, we derived an overall rate constant assuming the steady-state approximation for all intermediates (see the Supporting Information for the derivation). The overall second order rate constant is

$$k = \frac{k_1 k_2 k_3}{k_{-1}(k_{-2} + k_3) + k_2 k_3} \approx \frac{k_1 k_2 k_3}{k_{-1}(k_{-2} + k_3)} \quad (1)$$

where k_i and k_{-i} are the forward and reverse rate constants, respectively, for the ith step in the reaction pathway. The rate

constants for each step were evaluated using transition state theory[35] as

$$k_i = \frac{k_B T}{h c^0} e^{\Delta^{\ddagger} G_i / RT} \quad (2)$$

where $\Delta^{\ddagger} G_i$ is the free energy of activation, $k_B T$ is the thermal energy (T = 298.15 K), R is the gas constant, h is Planck's constant, and c^0 is the standard concentration (c^0 = 1 mol dm^{-3} for steps 1 and 2; c^0 = 1 for step 3). Evaluation of eq 1 according to the individual values of the rate constants (see Table 1) results in an overall second-order rate constant of 5.9 M^{-1} s^{-1}, in very good agreement with the experimental result (13 M^{-1} s^{-1}). Considering that many steps are involved in the

Table 1. Reaction Energies, Activation Free Energy Barriers, and Rate Constants Derived According to Eq 2

	C2−N$_\varepsilon$ distance (Å)	reaction energy (kcal/mol)	forward/backward activation energies (kcal/mol)	forward/backward rate constants
step 1	3.74	12.99	13.46/0.47	8.43 × 10^2 M^{-1} s^{-1}/ 2.81 × 10^{12} M^{-1} s^{-1}
step 2	1.58	−2.41	3.29/5.69	2.41 × 10^{10} M^{-1} s^{-1}/ 4.19 × 10^8 M^{-1} s^{-1}
step 3	1.51	−16.35	4.79	1.91 × 10^9 s^{-1}

reaction and that rate constants are exponentially dependent on activation energies, such agreement between theory and experiment is remarkable and partially validates the proposed structures and reaction pathway. This result further suggests that, in the overall process of binding between RKIP and locostatin (cavity recognition and chemical reaction), the reactive process is rate-determining. Furthermore, of all the reactive steps, the first one is clearly rate-determining.

Reacting and Nonreacting Conformations. As previously stated, the MD simulation and further refinements through QM/MM minimizations produced a ligand pose whose characteristics are consistent with the experimentally observed reactivity of the RKIP—locostatin complex. An important question to answer for an eventual ligand optimization is: What are the dominant characteristics in the cavity—ligand interaction, and what promotes reactivity? With these questions in mind, we list the following features: (1) Although locostatin is a potential hydrogen-bond acceptor, MD simulations reveal no hydrogen bond between the ligand and the surrounding amino acids. (2) The binding site of RKIP within 5 Å from the ligand, consisting of 15 amino acids, is charge-neutral. Thus, considering the charge neutrality of locostatin and the absence of hydrogen bonds, the stability of the protein—ligand complex is driven by shape complementarity and hydrophobicity. Two key residues, Tyr181 and Trp84, appear to play an important role in the recognition step. Accommodation of the ligand by the protein can be described mainly by π−π interactions arising from these aromatic residues. The phenyl ring of locostatin is oriented perpendicularly to the side chain of Tyr181 favoring a t-stacking configuration (Figure 5). This t-stacking arrangement is
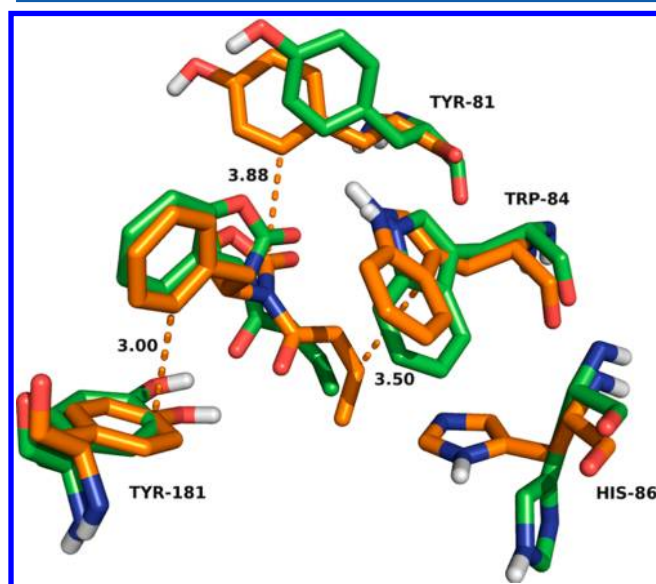

Figure 5. Snapshot of the first-step product and nonreactive conformation optimized at the B3LYP/lacvp*:OPLS2005 level of theory. Key aromatic residues are shown.

characterized by a contact distance of 3.88 Å defined as the shortest distance between one of the hydrogen atoms of locostatin's phenyl ring and a carbon atom in the Tyr181 ring. A similar interaction occurs with Trp84's rings and the sp^2 C3 carbon of locostatin. It is worth noting that a nearby residue, Tyr81, can potentially play a role similar to that of Tyr181, because it is placed in the outer part of the cavity (as is Tyr181)

and at a similar distance to His86. We suggest that new ligand designs that exploit these two interactions (with Tyr181 and Tyr81) simultaneously could lead to enhanced affinity. Addition of a methylbenzene at the C10 position, for instance, would force the interaction with these two residues.

The relative positioning of locostatin with respect to the mentioned residues remained almost constant throughout the MD simulations. However, the simulation revealed two distinct states, one reactive and the other nonreactive. These two states are characterized by two different rotamers of the side chain of His86. In the reactive state, the C−C$_\alpha$−C$_\beta$−C$_\gamma$ dihedral angle of His86 is around 150°, whereas in the nonreactive state, it remains around 60°, which is the starting value for the RKIP—phosphotyrosine X-ray crystal structure (2QYQ). The shortening of the distance between the two reactive groups is, therefore, a consequence of the movement of His86 toward locostatin (through side-chain rotation), rather than the movement of locostatin toward His86. Consequently, the nonreactive state is characterized by a side-chain conformation of His86 that keeps the nitrogen atom away from locostatin, leaving the latter still anchored to the cavity in a position similar to that in the reactive state.

CONCLUSIONS

We have presented an atomistic study to describe the interactions and reactivity between Raf-1 kinase inhibition protein (RKIP) and its small-molecule inhibitor locostatin. This reaction is initiated by the attack of the nitrogen (N$_\varepsilon$) of His86 on the carbon (C2) of locostatin and leads to the formation of an RKIP—butyrate adduct after hydrolysis. Of all reaction steps, the first step was found to be rate-limiting and presents a paradigm of a late transition state reaction. The reaction proceeds further, thermodynamically driven, through a hydrogen abstraction step from a solvent water molecule by the C3 atom. The final step of the reaction is hydrolysis, which was also found to be thermodynamically driven.

The results on the reactivity steps reported in this study show the ability of the hybrid QM/MM approach to credibly model the entire chemical reaction of large bimolecular complexes. We have identified several key features concerning ligand—cavity interactions during recognition and subsequent reactivity. The results are in a good agreement with published experimental findings and provide a detailed atomistic evaluation of RKIP—locostatin complex formation. In particular, the results suggest that the rate-limiting step is the reactivity process and not the recognition process, a question that has proved difficult to answer through the use of experimental or other theoretical methods.

Although the present effort mainly pertains to the mechanism of locostatin, this information might be useful in developing more reactive analogues. The conventional wisdom in drug design is that reactive inhibitors are undesirable; however, practice shows that this is not the case at all, as many drugs react specifically with a limited number of therapeutic targets. Therefore, in combination with future efforts to define the basis of the specificity of the recognition interaction and reactivity, what this study shows will be very useful in developing more potent analogs.

ASSOCIATED CONTENT

Ⓢ Supporting Information

Generation and analysis of locostatin conformers, criteria for docking pose selection, comparison between the computed

pose and that of the cocrystallized phosphotyrosine, ESP charge analysis after the formation of the first product, overall rate constant derivation, and MD simulation descriptors. This material is available free of charge via the Internet at http://pubs.acs.org.

■ AUTHOR INFORMATION

Corresponding Author
*E-mail: jose.gascon@uconn.edu.

Notes
The authors declare no competing financial interest.

■ ACKNOWLEDGMENTS

■ REFERENCES

(1) Yeung, K.; Janosch, P.; McFerran, B.; Rose, D. W.; Mischak, H.; Sedivy, J. M.; Kolch, W. *Mol. Cell. Biol.* **2000**, *20*, 3079−85.

(2) Yeung, K. C.; Rose, D. W.; Dhillon, A. S.; Yaros, D.; Gustafsson, M.; Chatterjee, D.; McFerran, B.; Wyche, J.; Kolch, W.; Sedivy, J. M. *Mol. Cell. Biol.* **2001**, *21*, 7207−17.

(3) Lorenz, K.; Lohse, M. J.; Quitterer, U. *Nature* **2003**, *426*, 574−9.

(4) Corbit, K. C.; Trakul, N.; Eves, E. M.; Diaz, B.; Marshall, M.; Rosner, M. R. *J. Biol. Chem.* **2003**, *278*, 13061−8.

(5) Bazzi, M. D.; Youakim, M. a; Nelsestuen, G. L. *Biochemistry* **1992**, *31*, 1125−34.

(6) Bernier, I.; Tresca, J. P.; Jolles, P. *Biochim. Biophys. Acta* **1986**, *871*, 19−23.

(7) Atmanene, C.; Laux, A.; Glattard, E.; Muller, A.; Schoentgen, F.; Metz-Boutigue, M.-H.; Aunis, D.; Van Dorsselaer, A.; Stefano, G. B.; Sanglier-Cianférani, S.; Goumon, Y. *Med. Sci. Monit.* **2009**, *15*, BR178−187.

(8) Yeung, K.; Seitz, T.; Li, S.; Janosch, P.; McFerran, B.; Kaiser, C.; Fee, F.; Katsanakis, K. D.; Rose, D. W.; Mischak, H.; Sedivy, J. M.; Kolch, W. *Nature* **1999**, *401*, 173−177.

(9) Park, S.; Yeung, M. L.; Beach, S.; Shields, J. M.; Yeung, K. C. *Oncogene* **2005**, *24*, 3535−3540.

(10) Trakul, N.; Menard, R. E.; Schade, G. R.; Qian, Z.; Rosner, M. R. *J. Biol. Chem.* **2005**, *280*, 24931−24940.

(11) Yuasa, H.; Ojika, K.; Mitake, S.; Katada, E.; Matsukawa, N.; Otsuka, Y.; Fujimori, O.; Hirano, A. *Brain Res. Dev. Brain Res.* **2001**, *127*, 1−7.

(12) Sultana, R.; Perluigi, M.; Butterfield, D. A. *Acta Neuropathol.* **2009**, *118*, 131−150.

(13) Hepler, D. J.; Wenk, G. L.; Cribbs, B. L.; Olton, D. S.; Coyle, J. T. *Brain Res.* **1985**, *346*, 8−14.

(14) Simister, P. C.; Burton, N. M.; Brady, R. L. *Forum Immunopathol. Dis. Ther.* **2011**, *2*, 59−70.

(15) Shevde, L. *Cancer Lett.* **2003**, *198*, 1−20.

(16) Kroslak, T.; Koch, T.; Kahl, E.; Höllt, V. *J. Biol. Chem.* **2001**, *276*, 39772−8.

(17) Keller, E. T.; Fu, Z.; Brennan, M. *J. Cell. Biochem.* **2005**, *94*, 273−8.

(18) Zhu, S.; Mc Henry, K. T.; Lane, W. S.; Fenteany, G. *Chem. Biol.* **2005**, *12*, 981−991.

(19) Mc Henry, K. T.; Ankala, S. V.; Ghosh, A. K.; Fenteany, G. *ChemBioChem* **2002**, *11*, 1105−1111.

(20) Beshir, A. B.; Argueta, C. E.; Menikarachchi, L. C.; Gascón, J. A.; Fenteany, G. *Forum Immunopathol. Dis. Ther.* **2011**, *2*, 47−58.

(21) Shemon, A. N.; Eves, E. M.; Clark, M. C.; Heil, G.; Granovsky, A.; Zeng, L.; Imamoto, A.; Koide, S.; Rosner, M. R. *PloS One* **2009**, *4*, e6028.

(22) *Maestro*, version 9.2; Schrödinger, LLC: New York, 2011.

(23) *Glide*, version 5.0; Schrödinger, LLC: New York, 2011.

(24) Friesner, R. A.; Banks, J. L.; Murphy, R. B.; Halgren, T. A.; Klicic, J. J.; Mainz, D. T.; Repasky, M. P.; Knoll, E. H.; Shelley, M.; Perry, J. K.; Shaw, D. E.; Francis, P.; Shenkin, P. S. *J. Med. Chem.* **2004**, *47*, 1739−49.

(25) Halgren, T. A.; Murphy, R. B.; Friesner, R. A.; Beard, H. S.; Frye, L. L.; Pollard, W. T.; Banks, J. L. *J. Med. Chem.* **2004**, *47*, 1750−9.

(26) Friesner, R. A.; Murphy, R. B.; Repasky, M. P.; Frye, L. L.; Greenwood, J. R.; Halgren, T. A.; Sanschagrin, P. C.; Mainz, D. T. *J. Med. Chem.* **2006**, *49*, 6177−96.

(27) Park, M.-S.; Gao, C.; Stern, H. A. *Proteins* **2010**, *79*, 304−14.

(28) *Qsite* 5.7, version 5.7; Schrödinger, LLC: New York, 2011.

(29) Shivakumar, D.; Williams, J.; Wu, Y.; Damm, W.; Shelley, J.; Sherman, W. *J. Chem. Theory Comput.* **2010**, *6*, 1509−1519.

(30) Guo, Z.; Mohanty, U.; Noehre, J.; Sawyer, T. K.; Sherman, W.; Krilov, G. *Chem. Biol. Drug Des.* **2010**, *75*, 348−59.

(31) *Maestro-Desmond Interoperability Tools*, version 3.0; Schrödinger: New York, 2011.

(32) Jorgensen, W. L.; Chandrasekhar, J.; Madura, J. D.; Impey, R. W.; Klein, M. L. *J. Chem. Phys.* **1983**, *79*, 926.

(33) Jorgensen, W. L.; Tirado-Rives, J. *J. Am. Chem. Soc.* **1988**, *110*, 1657−1666.

(34) Jorgensen, W. L.; Maxwell, D. S.; Tirado-Rives, J. *J. Am. Chem. Soc.* **1996**, *118*, 11225−11236.

(35) McQuarrie, D. A.; Simon, J. D. *Physical Chemistry: A Molecular Approach*; McGuire, A., Ed.; University Science Books, 1997; p 1270.